Chinese Chemical Letters 33 (2022) 2923–2927

Contents lists available at ScienceDirect

Chinese Chemical Letters

journal homepage: www.elsevier.com/locate/cclet

Three quinolizidine dimers from the seeds of *Sophora alopecuroides* and their hepatoprotective activities

Xiang Yuan, Jianshuang Jiang, Yanan Yang, Xu Zhang, Ziming Feng, Peicheng Zhang*

State Key Laboratory of Bioactive Substance and Function of Natural Medicines, Institute of Materia Medica, Chinese Academy of Medical Sciences & Peking Union Medical College, Beijing 100050, China

ARTICLE INFO

Article history:
Received 31 August 2021
Revised 11 October 2021
Accepted 26 October 2021
Available online 2 November 2021

Keywords:
Alkaloids
Sophora alopecuroides
X-ray diffraction
Hepatoprotective activities

ABSTRACT

Sophoralines A–C, three novel [2 + 2] cycloaddition dimers of matrine-based alkaloids with an unprecedented 6/6/6/6/4/6/6/6/6 nonacyclic skeleton containing 11 stereogenic centers, were isolated from *Sophora alopecuroides*. Their structures were determined by spectroscopic methods, and the absolute configurations were further determined by single-crystal X-ray diffraction analysis for **1** and quantum chemical calculations of electronic circular dichroism (ECD) spectra for **2** and **3**. Moreover, **1** exhibited excellent hepatoprotective activities in acetaminophen-induced liver injury *in vitro* and *in vivo*.

Sophora alopecuroides L. (Leguminosae) is widely distributed in northwestern China, and is commonly used as the traditional Chinese medicine "Kudouzi" for the treatment of eczema, sore throat, acute dysentery, and gastrointestinal hemorrhage [1—5]. Phytochemical investigations of *S. alopecuroides* have revealed that it contains large amounts of quinolizidine alkaloids. Since 1895, more than 50 alkaloids have been reported from *Sophora* species [6—9], and these alkaloids have been shown to exhibit anti-human immunodeficiency virus, antitumor, and hepatoprotective activities [10,11]. Among them, approximately 10 dimeric quinolizidine alkaloids, which are linked by a C–C or C–N single bond, have been identified. Recently, a number of studies on natural product dimers with structural diversity and pharmacological significance have been published, resulting in increased interest among various scientific communities [12—19]. In the present study, three new alkaloid dimers were isolated and identified from *S. alopecuroides*, namely sophoralines A–C (**1**–**3**), which represent the first [2 + 2] cycloaddition dimeric matrine-based alkaloid possessing an unprecedented 6/6/6/6/4/6/6/6/6 nonacyclic skeleton (Fig. 1). The biological studies showed that pretreatment with **1** markedly alleviated acetaminophen (APAP)-induced acute liver injury *via* inhibiting oxidative stress *in vitro* and *in vivo*.

Sophoraline A (**1**), colorless crystal (MeOH), was assigned its molecular formula $C_{30}H_{42}N_4O_2$ by the high resolution electrospray ionization mass spectroscopy (HRESIMS) ion at *m/z* 491.3382 $[M + H]^+$, suggesting 12 degrees of unsaturation. The characteristic infrared radiation (IR) absorption at 1666 cm^{-1} and UV absorption at 277 nm suggested the presence of an α,β-unsaturated amide group in **1**.

The ^1H nuclear magnetic resonance (NMR) spectrum of **1** exhibited the presence of two olefinic protons at δ_H 6.36 (dd, J = 10.0, 5.5 Hz) and 5.80 (d, J = 10.0 Hz) and two methylenes connected to heteroatoms at δ_H 4.25 (dd, J = 13.5, 4.5 Hz), 4.06 (dd, J = 13.5, 4.5 Hz), 3.07 (overlapped), and 2.65 (overlapped). The ^{13}C NMR and distortionless enhancement by polarization transfer (DEPT) spectra showed the existence of 30 carbons (Supporting information Table S1), including two carbonyls (δ_C 170.8 and 165.7), two sp^2 methines (δ_C 138.7 and 125.6), a quaternary carbon (δ_C 71.0), ten sp^3 methines (δ_C 64.1, 58.9, 53.2, 51.6, 51.3, 44.9, 39.6, 35.7, 32.8 and 27.6) and fifteen sp^3 methylene carbons (six of which were connected to heteroatom at δ_C 58.3, 58.2, 54.8, 45.5, 42.2 and 42.2). The carbonyls and double bond accounted for three degrees of unsaturation, indicating the presence of nine rings in the structure of **1**. The aforementioned spectroscopic evidences, particularly the molecular formula, suggested that **1** was likely a dimeric alkaloid.

Analysis of the ^1H–^1H correlation spectroscopy (COSY) spectrum aided by the heteronuclear single quantum correlation spectroscopy (HSQC) experiment led to the assignment of two isolated spin systems as depicted with bolded blue lines in Fig. 2. The heteronuclear multiple bond correlation spectroscopy (HMBC) cross peaks from H-14 to C-12 and C-15, H_2–17 to C-11 and C-15 indicated the presence of a δ-lactam. The planar structure of unit A was further constructed by the key correlations of H_2-17 to C-4, C-5 and C-6, and H-6 to C-2, C-5, C-7, C-11, and C-17, together with ^1H–^1H COSY correlations of H_2-2/H_2-3/H_2-4/H-5/H-6/H-7/H_2-

* Corresponding author.
E-mail address: pczhang@imm.ac.cn (P. Zhang).

https://doi.org/10.1016/j.cclet.2021.10.085
1001-8417/

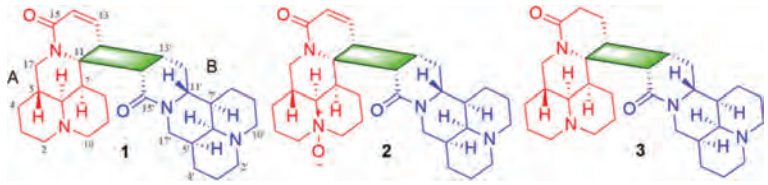

Fig. 1. Chemical structures of compounds **1**–**3**.

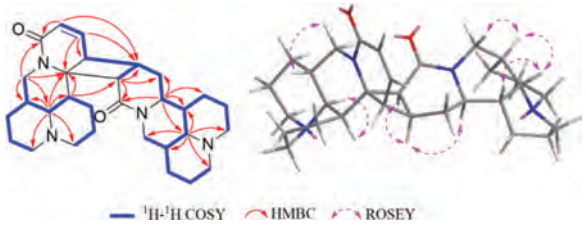

Fig. 2. Key ^{1}H–^{1}H COSY, HMBC, and ROESY correlations of **1**.

8/H_2-9/H_2-10, suggesting that unit A was similar to (−)-13,14-dehydrosophoridine [20]. The most notable difference was chemical shifts of C-7, C-11 and C-12 in (−)-13,14-dehydrosophoridine from δ_C 39.6, 53.5 and 29.9 to δ_C 51.6, 71.0 and 39.6, respectively, in unit A, caused by the formation of dimer. The unit B was subsequently established by the HMBC correlations of H-14′ to C-12′, C-13′ and C-15′, and H-11′ to C-6′, C-8′ and C-13′, together with H-6′ to C-2′, C-5′, C-7′, C-10′, C-11′ and C-17′. The HMBC correlations between H-12 and C-12′, C-13′, H-13 and C-13′, and contiguous ^{1}H–^{1}H COSY correlations extending from H-14 to H-11′ distinctly confirmed the connection of units A and B *via* the C-12–C-13′ bond. Different from other reported alkaloid dimers, the 12 degrees of unsaturation immanent in the molecular formula of **1** and the aforementioned NMR data, which represent two moieties of the structure occupying 11 degrees of unsaturation suggested that the dimer should possess one additional ring structure. Three methine groups (δ_C 51.3, 39.6 and 32.8) and a quaternary carbon (δ_C 71.0) were observed in **1**, as well as the key HMBC correlations from H-13 to C-12 and C-13′, H-12 to C-12′, C-13′ and C-14′, and H-7 to C-11 and C-14′, indicating that unit A is linked to unit B *via* a four-membered ring.

The rotating frame overhauser effect spectroscopy (ROESY) experiment was used to assign the relative configurations of the stereocenters in **1**. In unit A, ROESY correlations of H-5/H-17b, H-6/H-7 and H-6/H-17a (Fig. 2) indicate that H-6 and H-7 were the same oriented, whereas H-5 was assigned to the opposite side. In unit B, the ROESY correlations of H-13′/H-12, H-13′/H-11′ and H-13′/H-14′ for unit B demonstrated that H-12, H-11′, H-13′ and H-14′ were cofacial. Furthermore, the ROESY correlations of H-6′/H-5′ and H-6′/H-7′ suggest that H-5′, H-6′ and H-7′ have the same spatial orientation. Ultimately, the single crystal X-ray diffraction research was undertaken to elucidate the absolute configurations. The absolute configurations of **1** were unambiguously confirmed by X-ray diffraction with a Flack parameter of 0.02 (8). Finally, the result was confirmed through a comparison of the calculated and experimental electronic circular dichroism (ECD) spectra (Fig. 3). Therefore, the absolute configurations of **1** were determined as 5*R*,6*S*,7*S*,11*S*,12*R*,5′*S*,6′*S*,7′*R*,11′*R*,13′*S*,14′*S* and named sophoraline A.

Sophoraline B (**2**) was assigned its molecular formula $C_{30}H_{42}N_4O_3$ by the HRESIMS ion at *m/z* 507.3326 $[M + H]^+$. Detailed analyses of the molecular formula and NMR data in **2** possessed an extra "O" in comparison to that of **1**. Regardless of the stereochemistry, this indicated that **2** might be an oxidation congener of **1**. This speculation was confirmed by the ^{1}H–^{1}H COSY spectrum that exhibited the same spin systems as **1** (Fig. S3 in Supporting information). The chemical shifts of C-2, C-6

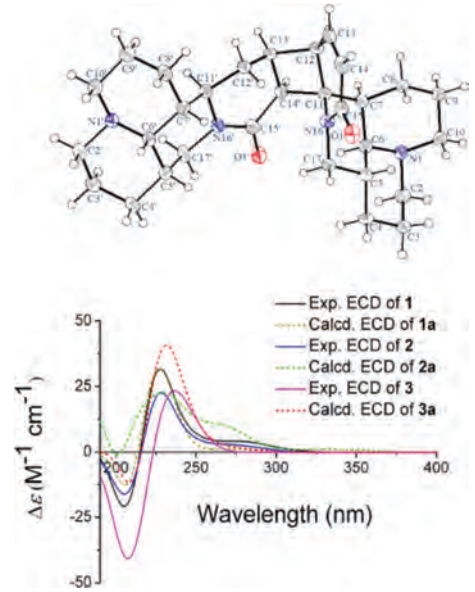

Fig. 3. Oak ridge thermal ellipsoid plot diagram of **1** and experimental and calculated ECD spectra of **1**–**3**.

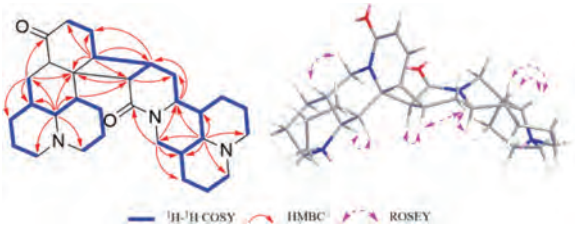

Fig. 4. Key ^{1}H–^{1}H COSY, HMBC and ROESY correlations of **3**.

and C-10 from δ_C 54.8, 58.9 and 45.5 in **1** to 71.5, 73.7 and 57.8 in **2**, respectively, suggested that unit A was *N*-oxide congener. Further interpretation of the HMBC correlation peaks were used to construct the planar architectural structure of **2** (Fig. 1).

The relative conformation of **2** was deduced based on biosynthetic pathway and ROESY experiment referencing to those of **1**. The correlations of H-5/H-17b, H-6/H-7 and H-17a, H-6′/H-5′ and H-7′, and H-13′/H-11′ suggested that **2** shared the same relative conformation of **1**. Furthermore, similar Cotton effects in the experimental circular dichroism (CD) spectra of the two compounds indicated that they may share the same absolute configurations. To further confirm its absolute configurations, calculated ECD spectrum of **2a** was compared with experimental data (Fig. 3), which eventually determined the absolute configurations of **2** to be 5*R*,6*S*,7*S*,11*S*,12*R*,5′*S*,6′*S*,7′*R*,11′*R*,13′*S*,14′*S* and named sophoraline B.

Sophoraline C (**3**) was assigned its molecular formula $C_{30}H_{44}N_4O_2$ by the HRESIMS ion at *m/z* 493.3526 $[M + H]^+$, suggesting 11 degrees of unsaturation. Further analyses of the molecular formula and NMR data of **3** also indicated that **3** showed highly similar planar structure as **1**. In comparison with the spectra of **1**, the upfield movement of C-13 and C-14 from δ_C 138.7 and 125.6 to δ_C 31.1 and 22.4 in **3**, respectively, suggesting

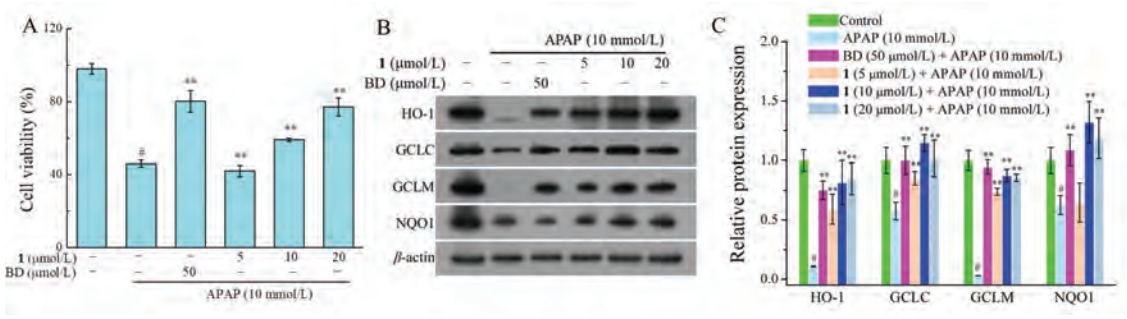

Fig. 5. Effects of **1** on APAP-induced liver injury. (A) Hepatoprotective effect of **1** on APAP-induced HepG2 cells. (B, C) Effects of **1** on oxidative stress protein expression in APAP-induced HepG2 cells. Values are the mean ± SD of three independent experiments. $^{\#}P < 0.05$, compared with the control group; $^{**}P < 0.01$ compared with the APAP group.

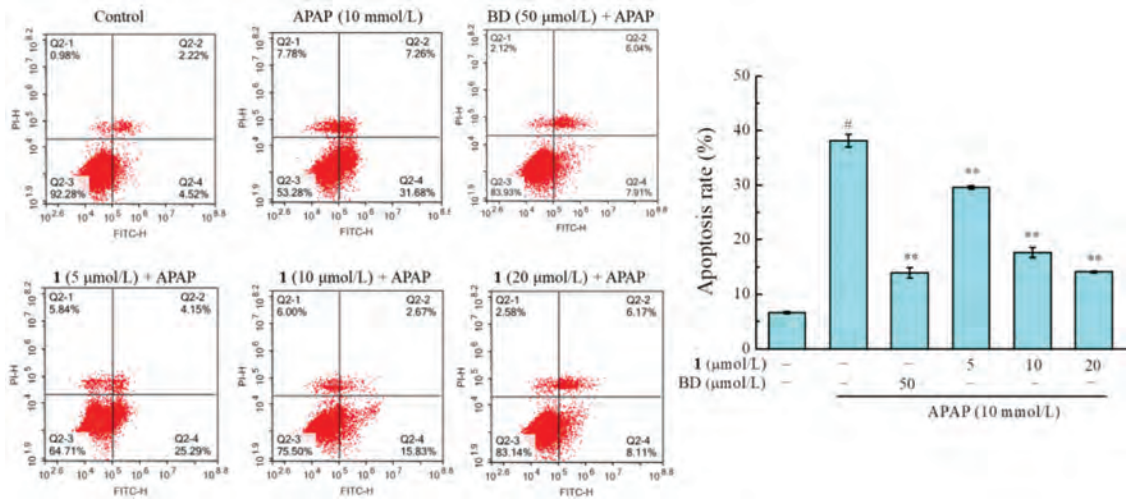

Fig. 6. Effects of **1** on APAP-induced apoptosis in HepG2 cells. HepG2 cells were pretreatment with 5, 10 and 20 μmol/L of **1** for 2 h, and subsequently incubated with APAP (10 mmol/L) for 24 h. Qualification of apoptosis rate was determined by flow cytometry using an Annexin V-FITC/PI double staining. Data were expressed as mean ± SD, $n = 3$ for each group, $^{\#}P < 0.05$ compared with the control group, $^{**}P < 0.01$ compared with the APAP group.

that the double bond is saturated. Based on the ^{1}H–^{1}H COSY spectrum correlations, a complicated spin system was observed in **3** (Fig. 4). The HMBC correlations from H-6′ to C-2′, C-5′, C-7′, C-10′, C-11′ and C-17′, as well as from H-11′ to C-6′, C-7′, C-12′ and C-13′ suggested that the planar structure of unit B was similar to that of **1**. Together with the HMBC correlations from H-6 to C-2, C-5, C-7, C-10, C-11 and C-17, as well as from H-12 to C-7, C-11, C-13 and C-14 determined a planar structure of unit A. Finally, two moieties are linked to form a four-membered ring system, which supported by the key HMBC correlations from H-7 to C-11 and C-14′, H-12 to C-13′ and C-14′, H-13′ to C-12 and C-13. The planar structure of **3** was unambiguously established as shown in Fig. 1.

The ROESY correlations of H-5/H-17b, H-6/H-7, H-6′/H-5′ and H7′, H-12/H-13′, H-13′/H-14′ and H-14′/H-11′, suggested that **3** shared the same relative conformation of **1**. The absolute configuration of **3** was also established by comparison of the experimental and calculated ECD spectra (Fig. 3), allowing assignment of the absolute configurations as 5*R*,6*S*,7*S*,11*S*,12*R*,5′*S*,6′*S*,7′*R*,11′*R*,13′*S*,14′*S*, and named sophoraline C.

Three novel [2 + 2] cycloaddition dimers of matrine-based alkaloids, with an unprecedented 6/6/6/6/4/6/6/6/6 nonacyclic skeleton containing 11 stereogenic centers, were isolated from the seeds of *S. alopecuroides*. These compounds represent the first example of an unusual pattern of [2 + 2] dimerization between two matrine-type alkaloids with highly fused polycyclic carbon skeletons. A plausible biosynthetic pathway is proposed in Scheme 1. The [2 + 2] cycloaddition reaction between two moieties is a key step in biosynthesis of **1**–**3**. Quinolizidine alkaloid may originate *via* the lysine pathway [21]. *In vivo*, **1** with tension cyclobutane structure could be formed from intermolecular [2 + 2] cycloaddition of two our previous isolated compounds, neosophocarine and sophoramine, by enzymatic processes. Furthermore, **1** could be oxidized to yield **2** and hydrogenated to obtain **3**.

Although the discovery of **1**–**3** has aroused great interest, it also raises the question whether they are natural products or handling artifacts. Thus, neosophocarine and sophoramine were performed for attempting [2 + 2] cycloaddition reactions under different conditions with heat, ultraphonic and UV, *etc*., while no dimers were detected (see Supporting information).

Furthermore, the hepatoprotective effect of **1** against APAP-induced hepatotoxicity in HepG2 cells and a mice model were evaluated. All animal experiments were approved by the Animal Experimentation Ethics Committee of Chinese Academy of Medical Sciences in complete compliance with the guidelines of Institutional Animal Care and Use Committees of Chinese Academy of Medical Sciences (Beijing, China). In the *in vitro* experiment, **1** could alleviate damage to the hepatocyte induced by APAP in HepG2 cells. As shown in Fig. 5A, the viability of HepG2 cells was significantly decreased by 46.21% after exposure to 10 mmol/L APAP. However, cells were pretreated with **1** significantly against APAP-induced cell damage, and increased cells viability to 77.50%. The flow cytometry results showed that **1** inhibited cell apoptosis and the intracellular reactive oxygen species (ROS) levels in APAP-induced HepG2 cells in a dose-dependent manner (Figs. 6

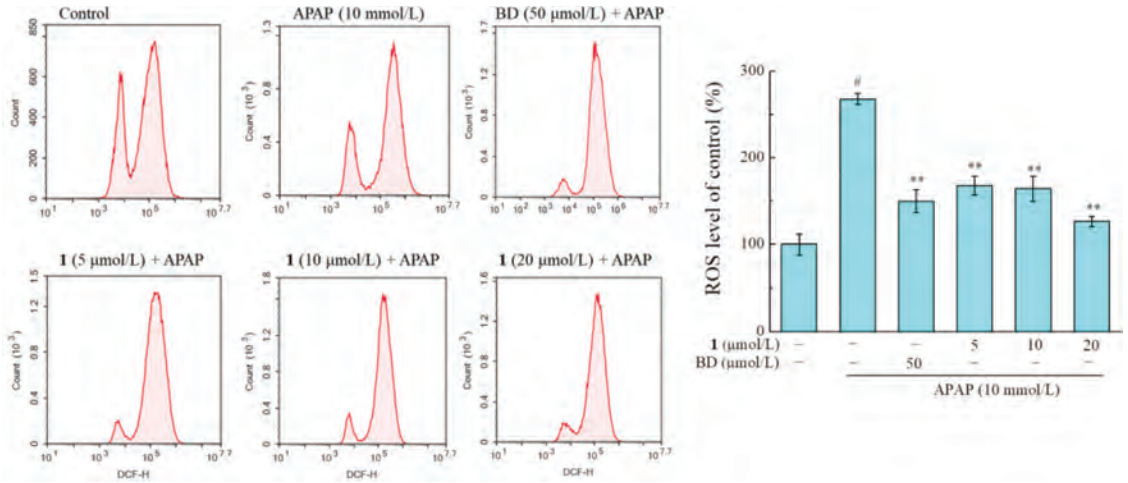

Fig. 7. Effects of **1** on APAP-induced elevate of intracellular ROS in HepG2 cells. Cells were pretreated with indicated concentrations of **1** for 2 h and then oxidative stress was stimulated by addition of APAP for 24 h. Intracellular ROS level analyzed by DCFDA staining. Data were expressed as mean ± SD, $n = 3$ for each group, $^{\#}P < 0.05$ compared with the control group, $^{**}P < 0.01$ compared with the APAP group.

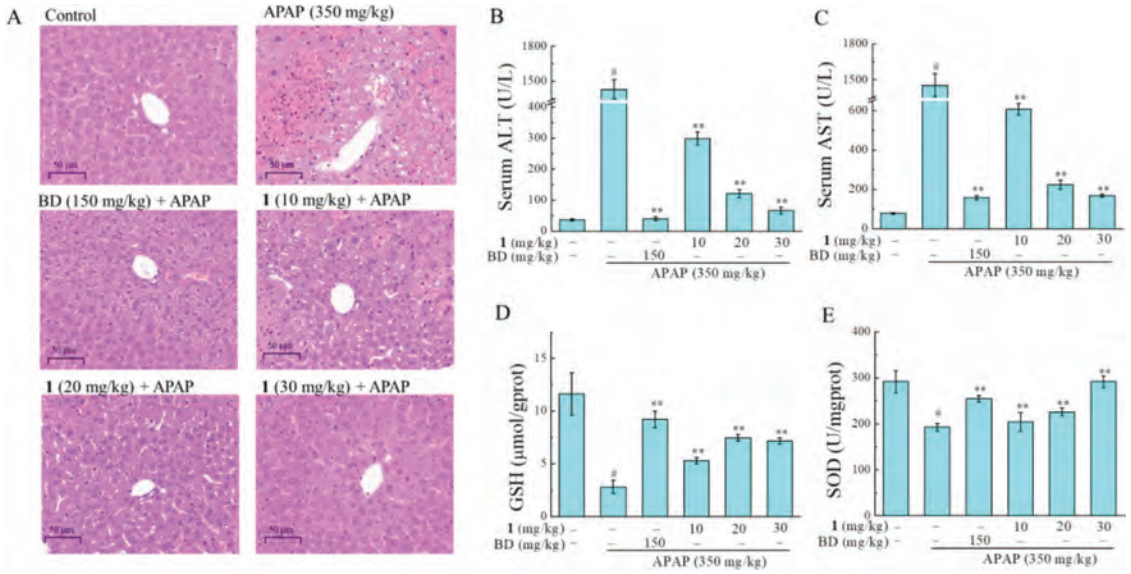

Fig. 8. Compound **1** ameliorated APAP-induced ALI in mice. (A) Histopathology of the mice liver sections (hematoxylin-eosin staining, original magnification of ×40). BD, bifendate. Effects of **1** on the serum levels of ALT (B), AST (C), and the hepatic levels of GSH (D), SOD (E) in APAP-induced ALI mice. Scale bar: 50 μm. Values are the mean ± SD of three independent experiments. $^{\#}P < 0.05$, compared with the control group; $^{**}P < 0.01$ compared with the APAP group.

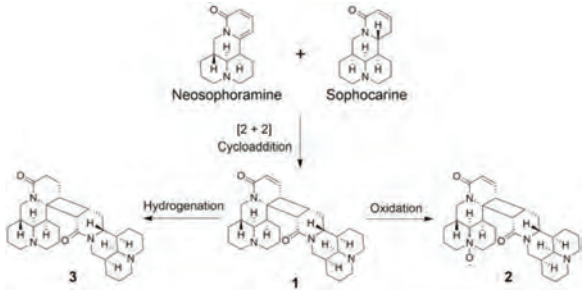

Scheme 1. Plausible biosynthetic pathway of **1**–**3**.

and 7). The down-regulation expression of oxidative stress proteins, heme oxygenase-**1** (HO-**1**), NAD(P)H dehydrogenase quinone **1** (NQO-**1**), and catalytic or modify subunit of glutamate-cysteine ligase (GCLC/GCLM), was markedly reversed by the pretreatment of **1**. To assess the protective effects of **1** *in vivo*, a mice model with acute liver injury (ALI) induced by APAP administration was established. As shown in Fig. 7, the levels of serum alanine transaminase (ALT) and aspartate transaminase (AST) in the APAP group sharply increased to 1429.22 ± 82.84 and 1455.47 ± 97.41 U/L, respectively, compared with 36.17 ± 2.96 and 78.37 ± 4.56 U/L in the control group. Pretreatment with **1** (10, 20 and 30 mg/kg) significantly attenuated APAP-induced elevation of ALT and AST levels in a dose-dependent manner. ALT activities decreased to 298.95 ± 20.26, 120.75 ± 13.42, and 66.35 ± 11.03 U/L when pretreated with 10, 20, and 30 mg/kg of **1**, respectively, and AST activities decreased to 608.55 ± 29.90, 224.95 ± 23.42 and 169.70 ± 8.67 U/L, respectively. In addition, the APAP-induced hepatic glutathione (GSH) and superoxide dismutase (SOD) depletion (2.80 ± 0.62 μmol/g protein and 192.39 ± 8.23 U/mg protein, respectively) was significantly prevented by pretreatment with **1** at 30 mg/kg (GSH levels increased to 7.16 ± 0.31 μmol/g protein and SOD levels increased to 291.56 ± 13.01 U/mg protein). An evaluation of liver provided

further evidence that pretreatment with **1** reversed APAP-induced hepatocellular necrosis, hemorrhaging, and infiltration of inflammatory cells (Fig. 8).

Declaration of competing interest

The authors declare no competing financial interest.

Acknowledgments

This work was supported by grants from the National Natural Science Foundation of China (No. 82104032), CAMS Innovation Fund for Medical Sciences (No. 2016-I2M-1–010), and the Drug Innovation Major Project (No. 2018ZX09711001–008).

Supplementary materials

Supplementary material associated with this article can be found, in the online version, at doi:10.1016/j.cclet.2021.10.085.

References

[1] C.L. Fan, Y.B. Zhang, Y. Chen, et al., J. Nat. Prod. 82 (2019) 3227–3232.
[2] Y.Q. Jia, Z.W. Yuan, X.S. Zhang, et al., J. Ethnopharmacol. 255 (2020) 112775.
[3] P. Xiao, J. Li, H. Kubo, et al., Chem. Pharm. Bull. 44 (1996) 1951–1953.
[4] A.U. Atta-Ur-Rahman, M.I. Choudhary, K. Parvez, et al., J. Nat. Prod. 63 (2000) 190–192.
[5] J. Kwon, S. Basnet, J.W. Lee, et al., Bioorg. Med. Chem. Lett. 25 (2015) 3314–3318.
[6] P.C. Plugge, Arch. Pharm. 233 (1895) 441–443.
[7] Y.B. Zhang, D. Luo, L. Yang, et al., J. Nat. Prod. 81 (2018) 2259–2265.
[8] Y.B. Zhang, X.L. Zhang, N.H. Chen, et al., Org. Lett. 19 (2017) 424–427.
[9] Y.B. Zhang, L. Yang, D. Lu, et al., Org. Lett. 20 (2018) 5942–5946.
[10] Y. Li, G. Wang, J. Liu, et al., Eur. J. Med. Chem. 188 (2020) 111972.
[11] Y.X. Huang, G. Wang, J.S. Zhu, et al., Eur. J. Inflamm. 14 (2016) 128–132.
[12] X. Liu, J. Yang, J. Fu, et al., Org. Lett. 21 (2019) 5753–5756.
[13] Y.B. Zhang, L.Q. Zhan, G.Q. Li, et al., J. Org. Chem. 81 (2016) 6273–6280.
[14] M. Bae, J.S. An, E.S. Bae, et al., Org. Lett. 21 (2019) 3635–3639.
[15] W.B. Han, G.Y. Wang, J.J. Tang, et al., Org. Lett. 22 (2020) 405–409.
[16] Y.L. Wang, Y.S. Ye, W.W. Fu, et al., Org. Lett. 21 (2019) 1534–1537.
[17] F.L. Li, S. Lin, S.T. Zhang, et al., Org. Lett. 21 (2019) 8353–8357.
[18] X.M. Chu, C. Wang, W. Liu, et al., Eur. J. Med. Chem. 161 (2019) 101–117.
[19] J.B. Xu, H. Zhang, L.S. Gan, et al., J. Am. Chem. Soc. 136 (2014) 7631–7633.
[20] I.S. Movsumov, E.A. Garaev, M.I. Isaev, Chem. Nat. Compd. 42 (2006) 116–117.
[21] P.M. Dewick , Medicinal Natural Products: A Biosynthetic Approach, John Wiley & Sons, West Sussex, 2002.